# Bidimensional study of the Maxwell-Bloch model in a nonlinear crystal

Olivier Saut

# Bidimensional study of the Maxwell-Bloch model in a nonlinear crystal

Olivier Saut *

**Abstract**

This article presents a numerical scheme for a model ([5]) of electromagnetic wave propagation in a nonlinear optical crystal in two dimensions in space. It uses Maxwell's equations to describe the wave field and Bloch's equations for the medium at the quantum-mechanical level. We have already described the discretization of the model in the unidimensional case in [14]. In this paper, we discretize the model in the bidimensional case, while ensuring a scheme of order 2. Finally, several numerical simulations are performed. We insist on physical effects that could not be observed with an unidimensional model.

**Keywords:** Nonlinear optics; Harmonic Generation; Quantum description of light and matter; Nonlinear optical crystal.

**PACS:** 42.65.An; 42.65.Ky; 42.50Ct; 42.70.Mp.

## 1 Introduction

To study the propagation of ultrashort laser pulses in nonlinear crystals, it has become necessary to develop models closer to the physics. Indeed, for such pulses, the response of the medium can not be assumed instantaneous. Thus, most classical models in nonlinear optics like systems of nonlinear Schrödinger equations [2, 12] are no longer valid .

In [5], we have described a Maxwell-Bloch model appropriate for nonlinear crystals. This model was compared to several macroscopic models and proved to be more accurate when studying wave-matter interaction in [7]. In this model, the electromagnetic field is described classically by the Maxwell equations in the time domain. We shall model the interaction of the electromagnetic field with

*Institut de Mathématiques, Université Bordeaux 1, CNRS UMR 5254 and INRIA Futurs, 351 cours de la libération, 33405 Talence Cedex, France (Olivier.Saut@math.u-bordeaux1.fr).

the material medium by means of the Bloch equations at the quantum-mechanical level.

In [14], we have described a scheme for the Maxwell-Bloch model in anisotropic media in the unidimensional case (the wave-field depends only on one variable in space). However, with this unidimensional scheme, we can not study physical effects on the shape of the pulse such as the diffraction or the Kerr effect. In practical applications, these effects are important as they could, for instance, decrease the efficiency of second harmonic generation [16] or damage the crystal through the self-focusing [11] of the laser beam. These effects would be taken into account with a bidimensional model.

The organization of this paper is as follows: Section 2 quickly exposes the physical context and the Maxwell-Bloch model.

In Section 3, we shall start by recalling the classical Yee scheme providing a discretization scheme for the electromagnetic field in Maxwell equations. These equations also involve the density matrix. We then discretize the Bloch equations describing the matter evolution. Finally we discretize the polarization term relating the wave-field and the medium. Throughout the complete discretization of the Maxwell-Bloch equations, we try to highlight the methods used to ensure a second order scheme.

In Section 4, we describe the boundary conditions we have used to perform numerical simulations.

Eventually, in Section 5, we perform several numerical experimentations to check the validity of our model.

# 2 Physical context

## 2.1 Experimental setup

In this paper, let us consider the following experimental setup. A wave-field propagates in a linear medium, before traveling through a nonlinear crystal.

Figure 1: Experimental setup.

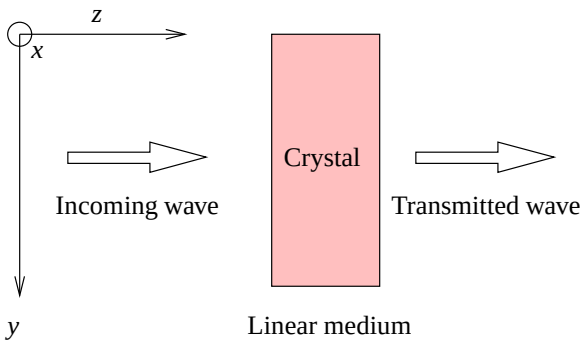


## 2.2 Maxwell Equations

The incoming plane wave is represented by the pair $(\mathbf{E},\mathbf{B})$, where $\mathbf{E}$ is the electric field and $\mathbf{B}$ the magnetic induction. The fields $\mathbf{E}$ and $\mathbf{B}$ obey the Maxwell equations:

$$\begin{cases} \dfrac{\partial \mathbf{B}}{\partial t} = -\text{rot}\,\mathbf{E}, \\ \dfrac{\partial \mathbf{E}}{\partial t} = \dfrac{1}{\mu_0}\varepsilon^{-1}\text{rot}\,\mathbf{B} - \varepsilon^{-1}\dfrac{\partial \mathbf{P}}{\partial t}, \\ \text{div}\,\mathbf{B} = 0, \\ \text{div}\,\mathbf{D} = 0, \end{cases} \tag{1}$$

where $\varepsilon$ is the static linear susceptibility tensor (*i.e.* a $3\times 3$ matrix) of the medium in which the wave travels. We recall that $\mathbf{D} = \varepsilon\mathbf{E} + \mathbf{P}$. From now, we denote by $\eta$ the tensor $\varepsilon^{-1}$.

As shown on Figure 1, the wave propagates along the direction $z$. We shall make the assumption that the fields $\mathbf{E}$ and $\mathbf{B}$ depend only of the two space variables $y$ and $z$. Then the previous system (1) can be developed as the Faraday equations governing the magnetic induction $\mathbf{B}$

$$\begin{cases} \partial_t B_x = -\partial_y E_z + \partial_z E_y, \\ \partial_t B_y = -\partial_z E_x, \\ \partial_t B_z = \partial_y E_x, \end{cases} \tag{2}$$

and the Ampere equations leading the evolution of the electric field **E**,

$$\begin{cases} \partial_t E_x = & \frac{1}{\mu_0}[\eta_{xx}(\partial_y B_z - \partial_z B_y) + \eta_{xy}\partial_z B_x - \eta_{xz}\partial_y B_x] \\ & \qquad -[\eta\partial_t \mathbf{P}]_x, \\ \partial_t E_y = & \frac{1}{\mu_0}[\eta_{yx}(\partial_y B_z - \partial_z B_y) + \eta_{yy}\partial_z B_x - \eta_{yz}\partial_y B_x] \\ & \qquad -[\eta\partial_t \mathbf{P}]_y, \\ \partial_t E_z = & \frac{1}{\mu_0}[\eta_{zx}(\partial_y B_z - \partial_z B_y) + \eta_{zy}\partial_z B_x - \eta_{zz}\partial_y B_x] \\ & \qquad -[\eta\partial_t \mathbf{P}]_z, \end{cases} \tag{3}$$

Furthermore, as it was described in [6, 14], the referential in which the Maxwell equations are written, can be chosen to minimize the number of non-vanishing components of the tensor $\eta$. By choosing an adequate system of axes to describe the wave-field, we are then able to simplify the Ampere equations as

$$\begin{cases} \partial_t E_x &= \frac{1}{\mu_0}[\eta_{xx}(\partial_y B_z - \partial_z B_y) - \eta_{xz}\partial_y B_x] - [\eta\partial_t \mathbf{P}]_x, \\ \partial_t E_y &= \frac{1}{\mu_0}\eta_{yy}\partial_z B_x - [\eta\partial_t \mathbf{P}]_y, \\ \partial_t E_z &= \frac{1}{\mu_0}[\eta_{zx}(\partial_y B_z - \partial_z B_y) - \eta_{zz}\partial_y B_x] - [\eta\partial_t \mathbf{P}]_z, \end{cases} \tag{4}$$

The constitutive laws ($\operatorname{div}\mathbf{B} = \operatorname{div}\mathbf{D} = 0$) yield in the bidimensional case

$$\begin{cases} \partial_y B_y + \partial_z B_z = 0, \\ \partial_y D_y + \partial_z D_z = 0. \end{cases}$$

As equations (2) and (4) suffice to fully determine the electromagnetic field, these laws do not play any role in the sequel.

## 2.3 Bloch equations

The crystal is described at the quantum-mechanical level. This system evolves under the action of an Hamiltonian $\mathcal{H}$, classically decomposed in $\mathcal{H} = \mathcal{H}_0 + V$, $\mathcal{H}_0$ being the free Hamiltonian and $V$ the potential resulting from the action of the electromagnetic field. We make the assumption that the free Hamiltonian $\mathcal{H}_0$ has N distinct eigenvalues: $\mathcal{E}_1 = \hbar\omega_1, \ldots, \mathcal{E}_N = \hbar\omega_N$. For convenience, we write $\omega_{nm} = \omega_n - \omega_m$.

We do not assume that the quantum system is in a pure quantum state. Thus we shall use a statistical description of the system through the density matrix $\rho$ (see page 379 of [15] for instance). The diagonal elements of the density matrix represent the population levels of the corresponding eigenspace of the free Hamiltonian, while the off-diagonal terms represent the coherences between these levels.

It is straightforward (e.g. see [8, 11]) to show that the density matrix $\rho$ obeys the Bloch equations:

$$\partial_t \rho_{jk} = -i\omega_{jk}\rho_{jk} - \frac{i}{\hbar}[V,\rho]_{jk} \tag{5}$$

for all $1 \leq j,k \leq N$, where we recall $[A,B] = AB - BA$.

In the dipolar approximation, the potential $V$ is given by

$$V = -\mathbf{E}.\mu = -E_x\mu_x - E_y\mu_y - E_z\mu_z, \tag{6}$$

where $\mu$ is a square matrix of dimension $N^2$ whose coefficients are vectors in $\mathbb{C}^3$. The matrix $\mu$ is called the *dipolar matrix* and is computed from the eigenvectors of the free Hamiltonian and the position operator (see [8, 11] for instance). We denote by $\mu_x$, $\mu_y$ and $\mu_z$ the matrices obtained by taking one coordinate of each vector of $\mu$ (their coefficients are thus complex numbers).

To simplify the equations, we introduce the operator R defined by $\mathrm{R}(\rho)_{jk} = -i\omega_{jk}\rho_{jk}$.

The two sets of equations (1) and (5) are related by the polarization $\mathbf{P}$ which is given by

$$\mathbf{P} = \mathcal{N}\,\mathrm{tr}(\mu\rho), \tag{7}$$

where $\mathcal{N}$ is the density of molecules per unit volume.

Hence, equations (1), (5) and (7) form a closed system.

# 3 Discretization

In the previous section, we wrote the system of equations that we now intend to solve numerically. Before proceeding with numerical experimentations, we need a scheme for discretizing these equations.

## 3.1 Maxwell equations

To discretize the Maxwell equations, we adapt Yee's scheme [17, 18].

First, let us introduce a notation. Let $(a_{j,k})$ a sequel indexed by j and k. We define the finite differences operators:

$$(\mathbb{D}^y a)_{j,\cdot} = \frac{a_{j+\frac{1}{2},\cdot} - a_{j-\frac{1}{2},\cdot}}{\delta y},$$

for $j = j + \frac{1}{2}$, we clearly obtain,

$$(\mathbb{D}^y a)_{j+\frac{1}{2},\cdot} = \frac{a_{j+1,\cdot} - a_{j,\cdot}}{\delta y},$$

and along the $z$ direction,

$$(\mathbb{D}^z a)_{.,k} = \frac{a_{.,k+\frac{1}{2}} - a_{.,k-\frac{1}{2}}}{\delta z},$$
$$(\mathbb{D}^z a)_{.,k+\frac{1}{2}} = \frac{a_{.,k+1} - a_{.,k}}{\delta z}.$$

For the time derivatives, we also define,

$$(\mathbb{D}^t a)^n = \frac{a^{n+\frac{1}{2}} - a^{n-\frac{1}{2}}}{\delta t},$$
$$(\mathbb{D}^t a)^{n+\frac{1}{2}} = \frac{a^{n+1} - a^n}{\delta t}.$$

We define the average operator $\mathbb{A}$ by

$$(\mathbb{A}^y a)_{j,.} = \frac{a_{j+\frac{1}{2},.} + a_{j+\frac{1}{2},.}}{2},$$

using the same idea, we define $\mathbb{A}^z$ and $\mathbb{A}^{y,z}$ by

$$(\mathbb{A}^{y,z} a)_{j,k} = \frac{a_{j+\frac{1}{2},k+\frac{1}{2}} + a_{j-\frac{1}{2},k+\frac{1}{2}} + a_{j-\frac{1}{2},k-\frac{1}{2}} + a_{j+\frac{1}{2},k-\frac{1}{2}}}{4}.$$

Classically, we discretize the electric field $\mathbf{E}$ and the magnetic induction $\mathbf{B}$ shifted by half a step in time as in Figure 2.

The Faraday equations (2) do not depend on $\rho$, they are easily discretized:

$$\begin{aligned}
(\mathbb{D}^t B_x)^n_{j+\frac{1}{2},k+\frac{1}{2}} &= -(\mathbb{D}^y E_z)^n_{j+\frac{1}{2},k+\frac{1}{2}} + (\mathbb{D}^z E_y)^n_{j+\frac{1}{2},k+\frac{1}{2}} \\
(\mathbb{D}^t B_y)^n_{j,k+\frac{1}{2}} &= -(\mathbb{D}^z E_x)^n_{j,k+\frac{1}{2}} \\
(\mathbb{D}^t B_z)^n_{j+\frac{1}{2},k} &= (\mathbb{D}^y E_x)^n_{j+\frac{1}{2},k}
\end{aligned} \tag{8}$$

which gives us a scheme of order 2. Hence, given the electric field $\mathbf{E}^n$ at time $t^n = n\delta t$, we can compute the magnetic induction $\mathbf{B}^{n+\frac{1}{2}}$ at time $t^{n+\frac{1}{2}} = (n+\frac{1}{2})\delta t$.

Following the scheme of Figure 2, we then write the Ampere equations (4) for time $t^{n+\frac{1}{2}}$:

$$\begin{aligned}
(\mathbb{D}^t E_x)^{n+\frac{1}{2}}_{j,k} \quad = \quad & \frac{\eta_{xx}}{\mu_0}\left[(\mathbb{D}^y B_z)^{n+\frac{1}{2}}_{j,k} - (\mathbb{D}^z B_y)^{n+\frac{1}{2}}_{j,k}\right] - \frac{\eta_{xz}}{\mu_0}(\mathbb{D}^y B_x)^{n+\frac{1}{2}}_{j,k} \\
& -\eta_{xx}(\partial_t P_x)|^{n+\frac{1}{2}}_{j,k} - \eta_{xz}(\partial_t P_z)|^{n+\frac{1}{2}}_{j,k}.
\end{aligned} \tag{9}$$

According to Figure 2, the magnetic induction $B_x$ is only computed at the points $(j+\frac{1}{2}, k+\frac{1}{2})$. Hence, we have to approximate the value of $(\mathbb{D}^y B_x)^{n+\frac{1}{2}}_{j,k}$.

Figure 2: Modified Yee's scheme for discretizing the electromagnetic wave-fields and the density matrix ρ.

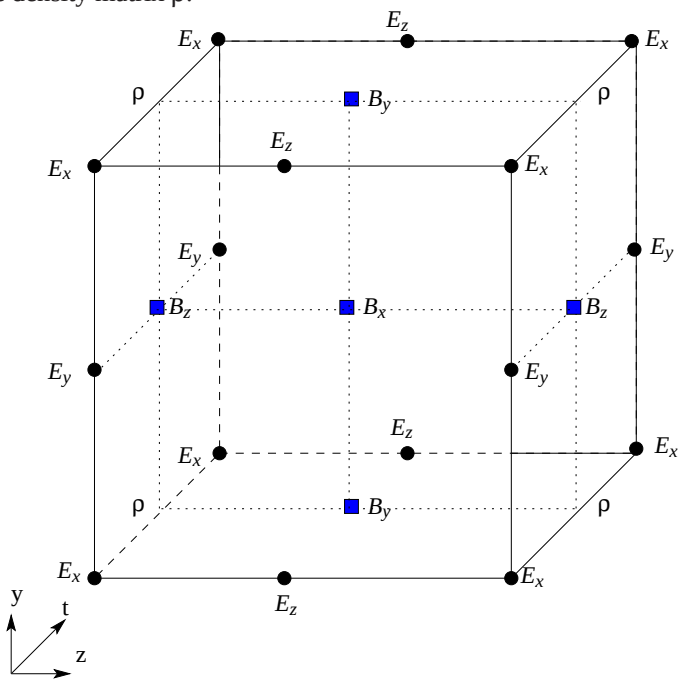

For this purpose, we use the following approximations (of order 2)

$$B_x|_{j+\frac{1}{2},k}^{n+\frac{1}{2}} \sim \frac{1}{2}\left(B_x|_{j+\frac{1}{2},k+\frac{1}{2}}^{n+\frac{1}{2}} + B_x|_{j+\frac{1}{2},k-\frac{1}{2}}^{n+\frac{1}{2}}\right),$$

$$B_x|_{j-\frac{1}{2},k}^{n+\frac{1}{2}} \sim \frac{1}{2}\left(B_x|_{j-\frac{1}{2},k+\frac{1}{2}}^{n+\frac{1}{2}} + B_x|_{j-\frac{1}{2},k-\frac{1}{2}}^{n+\frac{1}{2}}\right),$$

which give,

$$(\mathbb{D}^y B_x)_{j,k}^{n+\frac{1}{2}} \sim \frac{(\mathbb{D}^y B_x)_{j,k+\frac{1}{2}}^{n+\frac{1}{2}} + (\mathbb{D}^y B_x)_{j,k-\frac{1}{2}}^{n+\frac{1}{2}}}{2}. \tag{10}$$

Finally, we obtain the expression of $E_x|_{j,k}^{n+1}$:

$$\begin{aligned} E_x|_{j,k}^{n+1} = \quad & E_x|_{j,k}^{n} + \tfrac{\delta t}{\mu_0}\eta_{xx}\left[(\mathbb{D}^y B_z)_{j,k}^{n+\frac{1}{2}} - (\mathbb{D}^z B_y)_{j,k}^{n+\frac{1}{2}}\right] \\ & - \tfrac{\delta t}{2\mu_0}\eta_{xz}\left[(\mathbb{D}^y B_x)_{j,k+\frac{1}{2}}^{n+\frac{1}{2}} + (\mathbb{D}^y B_x)_{j,k-\frac{1}{2}}^{n+\frac{1}{2}}\right] \\ & - \eta_{xx}\delta t(\partial_t P_x)|_{j,k}^{n+\frac{1}{2}} - \eta_{xz}\delta t(\partial_t P_z)|_{j,k}^{n+\frac{1}{2}}. \end{aligned} \tag{11}$$

For the second component of the electric field $E_y$, the discretization is the same as in the isotropic case, that is to say,

$$(\mathbb{D}^t E_y)_{j+\frac{1}{2},k}^{n+\frac{1}{2}} = \frac{\eta_{yy}}{\mu_0}(\mathbb{D}^z B_x)_{j+\frac{1}{2},k}^{n+\frac{1}{2}} - \eta_{yy}(\partial_t P_y)|_{j+\frac{1}{2},k}^{n+\frac{1}{2}},$$

which yields

$$E_y|_{j+\frac{1}{2},k}^{n+1} = E_y|_{j+\frac{1}{2},k}^{n} + \frac{\delta t}{\mu_0}\eta_{yy}(\mathbb{D}^z B_x)_{j+\frac{1}{2},k}^{n+\frac{1}{2}} - \eta_{yy}\delta t(\partial_t P_y)|_{j+\frac{1}{2},k}^{n+\frac{1}{2}}. \tag{12}$$

We still have to compute the third component of **E**, which is given by

$$\begin{aligned} (\mathbb{D}^t E_z)_{j,k+\frac{1}{2}}^{n+\frac{1}{2}} = \quad & -\tfrac{\eta_{zz}}{\mu_0}\eta_{zz}(\mathbb{D}^y B_x)_{j,k+\frac{1}{2}}^{n+\frac{1}{2}} + \tfrac{\eta_{zx}}{\mu_0}\left[(\partial_y B_z)|_{j,k+\frac{1}{2}}^{n+\frac{1}{2}} - (\partial_z B_y)|_{j,k+\frac{1}{2}}^{n+\frac{1}{2}}\right] \\ & - \eta_{zx}(\partial_t P_x)|_{j,k+\frac{1}{2}}^{n+\frac{1}{2}} - \eta_{zz}(\partial_t P_z)|_{j,k+\frac{1}{2}}^{n+\frac{1}{2}}, \end{aligned}$$

according to the scheme of Figure 2.

To compute $(\partial_y B_z)|_{j,k+\frac{1}{2}}^{n+\frac{1}{2}}$, we use the approximation:

$$(\partial_y B_z)|_{j,k+\frac{1}{2}}^{n+\frac{1}{2}} \sim \frac{B_z|_{j+\frac{1}{2},k+1}^{n+\frac{1}{2}} + B_z|_{j+\frac{1}{2},k}^{n+\frac{1}{2}} - B_z|_{j-\frac{1}{2},k+1}^{n+\frac{1}{2}} - B_z|_{j-\frac{1}{2},k}^{n+\frac{1}{2}}}{2\delta y}.$$

We also have to estimate $(\partial_z B_y)|^{n+\frac{1}{2}}_{j,k+\frac{1}{2}}$. However, $B_y$ is only known on points of the kind $(j,k+\frac{1}{2})$.

We then use

$$(\partial_z B_y)|^{n+\frac{1}{2}}_{j,k+\frac{1}{2}} \sim \frac{B_y|^{n+\frac{1}{2}}_{j,k+1} - B_y|^{n+\frac{1}{2}}_{j,k}}{\delta z}$$

But, every term of the previous equation is also to be computed through

$$B_y|^{n+\frac{1}{2}}_{j,k+1} \sim \frac{1}{2}\left(B_y|^{n+\frac{1}{2}}_{j,k+\frac{1}{2}} + B_y|^{n+\frac{1}{2}}_{j,k+\frac{3}{2}}\right),$$

$$B_y|^{n+\frac{1}{2}}_{j,k} \sim \frac{1}{2}\left(B_y|^{n+\frac{1}{2}}_{j,k+\frac{1}{2}} + B_y|^{n+\frac{1}{2}}_{j,k-\frac{1}{2}}\right).$$

Finally, we obtain the expression of $E_z|^{n+1}_{j,k+\frac{1}{2}}$:

$$\begin{aligned} E_z|^{n+1}_{j,k+\frac{1}{2}} = \quad & E_z|^{n}_{j,k+\frac{1}{2}} - \frac{\delta t \eta_{zz}}{\mu_0}(\mathbb{D}^y B_x)^{n+\frac{1}{2}}_{j,k+\frac{1}{2}} - \frac{\delta t \eta_{zx}}{\mu_0}\left[\frac{B_y|^{n+\frac{1}{2}}_{j,k+\frac{3}{2}} - B_y|^{n+\frac{1}{2}}_{j,k-\frac{1}{2}}}{2\delta z}\right] \\ & + \frac{\delta t \eta_{zx}}{\mu_0}\frac{(\mathbb{D}^y B_z)^{n+\frac{1}{2}}_{j,k+1} + (\mathbb{D}^y B_z)^{n+\frac{1}{2}}_{j,k}}{2} \\ & - \eta_{zx}\delta t(\partial_t P_x)|^{n+\frac{1}{2}}_{j,k+\frac{1}{2}} - \eta_{zz}\delta t(\partial_t P_z)|^{n+\frac{1}{2}}_{j,k+\frac{1}{2}}. \end{aligned} \tag{13}$$

## 3.2 Bloch equations

The discretization of the Bloch equations (5) is the same as in the unidimensional case [14]. For the reader's convenience, we recall it briefly. We use a Strang splitting method. Each component of the Bloch equations is solved separately.

The part of the equation involving the free Hamiltonian is

$$\partial_t \rho_{jk} = -i\omega_{jk}\rho_{jk},$$

for all $1 \leq j,k \leq N$, which can easily be rewritten as a diagonal system. We shall call $S_{\mathcal{H}_0}$ the solving operator of this part of the splitting.

The interaction of the electric field $\mathbf{E}$ with the crystal is rendered by

$$\partial_t \rho = -\tfrac{i}{\hbar}[\mathbf{V},\rho]$$

which is solved with the analytical solution of the previous equation:

$$\rho(t) = e^{-\frac{i}{\hbar}\int_0^t V(s)ds}\rho(0)e^{+\frac{i}{\hbar}\int_0^t V(s)ds}.$$

We shall call $S_{\mathcal{H}}$, the solving operator of this part of the splitting. The complete discretization, which preserves the algebraic properties of the density matrix is described in [14].

As we wish to obtain an accurate overall scheme, we use a Strang method, which is of order 2. The density matrix is computed by

$$\rho^{n+\frac{1}{2}} = S_{\mathcal{H}_0}^{\frac{1}{2}} S_{\mathcal{H}} S_{\mathcal{H}_0}^{\frac{1}{2}} \rho^{n-\frac{1}{2}}. \tag{14}$$

## 3.3 Discretization of the polarization term

Up to now, we have used the classical scheme of Yee to discretize the wave-field. In this section, we will show how to discretize the polarization **P** to obtain a second order scheme.

The Ampere equations (4) involve the time-derivative of the polarization **P**.

Let us recall that the polarization $\mathbf{P} = (P_x, P_y, P_z)$ is given by

$$\begin{cases} P_x = \mathcal{N}\,\mathrm{tr}(\mu_x \rho), \\ P_y = \mathcal{N}\,\mathrm{tr}(\mu_y \rho), \\ P_z = \mathcal{N}\,\mathrm{tr}(\mu_z \rho). \end{cases}$$

To express the time-derivatives of the polarization, we use the Bloch equations (5). We have

$$\partial_t P_d = \mathcal{N}\,\mathrm{tr}(\mu_d \partial_t \rho),\ d \in \{x,y,z\},$$

then the Bloch equations give us

$$\partial_t P_d = \mathcal{N}\,\mathrm{tr}(\mu_d \mathrm{R}(\rho)) - \frac{i\mathcal{N}}{\hbar}\mathrm{tr}(\mu_d [V,\rho]),\ d \in \{x,y,z\}. \tag{15}$$

We shall now write inject this equation in equation (11) to compute $E_x|_{j,k}^{n+\frac{1}{2}}$. Equation (11) involves $(\partial_t P_x)|_{j,k}^{n+\frac{1}{2}}$ and $(\partial_t P_z)|_{j,k}^{n+\frac{1}{2}}$.

Using equation (15), we have

$$\begin{aligned} (\partial_t P_x)|_{j,k}^{n+\frac{1}{2}} &= \mathcal{N}\,\mathrm{tr}\,(\mu_x \mathrm{R}(\rho|_{j,k}^{n+\frac{1}{2}})) - \frac{i\mathcal{N}}{\hbar}\mathrm{tr}\,(\mu_x [V|_{j,k}^{n+\frac{1}{2}}, \rho|_{j,k}^{n+\frac{1}{2}}]), \\ (\partial_t P_z)|_{j,k}^{n+\frac{1}{2}} &= \mathcal{N}\,\mathrm{tr}\,(\mu_z \mathrm{R}(\rho|_{j,k}^{n+\frac{1}{2}})) - \frac{i\mathcal{N}}{\hbar}\mathrm{tr}\,(\mu_z [V|_{j,k}^{n+\frac{1}{2}}, \rho|_{j,k}^{n+\frac{1}{2}}]). \end{aligned}$$

The potential $V|_{j,k}^{n+\frac{1}{2}}$ is given by

$$V|_{j,k}^{n+\frac{1}{2}} = -\mu_x E_x|_{j,k}^{n+\frac{1}{2}} - \mu_y E_y|_{j,k}^{n+\frac{1}{2}} - \mu_z E_z|_{j,k}^{n+\frac{1}{2}},$$

where we take

$$E_x|_{j,k}^{n+\frac{1}{2}} \sim \frac{E_x|_{j,k}^{n+1} + E_x|_{j,k}^{n}}{2},$$
$$E_y|_{j,k}^{n+\frac{1}{2}} \sim \frac{E_y|_{j+\frac{1}{2},k}^{n+1} + E_y|_{j-\frac{1}{2},k}^{n+1} + E_y|_{j+\frac{1}{2},k}^{n} + E_y|_{j-\frac{1}{2},k}^{n}}{4},$$
$$E_z|_{j,k}^{n+\frac{1}{2}} \sim \frac{E_z|_{j,k+\frac{1}{2}}^{n+1} + E_z|_{j,k-\frac{1}{2}}^{n+1} + E_z|_{j,k+\frac{1}{2}}^{n} + E_z|_{j,k-\frac{1}{2}}^{n}}{4}.$$

The equation (12) on $E_y$ involves $(\partial_t P_y)|_{j+\frac{1}{2},k}^{n+\frac{1}{2}}$, which is computed as

$$(\partial_t P_y)|_{j+\frac{1}{2},k}^{n+\frac{1}{2}} = \mathcal{N}\,\mathrm{tr}(\mu_y \mathrm{R}(\rho|_{j+\frac{1}{2},k}^{n+\frac{1}{2}})) - \frac{i\mathcal{N}}{\hbar}\mathrm{tr}(\mu_y [V|_{j+\frac{1}{2},k}^{n+\frac{1}{2}}, \rho|_{j+\frac{1}{2},k}^{n+\frac{1}{2}}]).$$

The dipolar matrix on the points $(j+\frac{1}{2},k)$ is calculated by (an approximation of order 2)

$$\rho|_{j+\frac{1}{2},k}^{n+\frac{1}{2}} \sim \frac{\rho|_{j+1,k}^{n+\frac{1}{2}} + \rho|_{j,k}^{n+\frac{1}{2}}}{2},$$

the potential is given by

$$V|_{j+\frac{1}{2},k}^{n+\frac{1}{2}} = -\mu_x E_x|_{j+\frac{1}{2},k}^{n+\frac{1}{2}} - \mu_y E_y|_{j+\frac{1}{2},k}^{n+\frac{1}{2}} - \mu_z E_z|_{j+\frac{1}{2},k}^{n+\frac{1}{2}}.$$

The coordinates of the electric field are obtained from

$$E_x|_{j+\frac{1}{2},k}^{n+\frac{1}{2}} \sim \frac{E_x|_{j+1,k}^{n+1} + E_x|_{j,k}^{n+1} + E_x|_{j+1,k}^{n} + E_x|_{j,k}^{n}}{4},$$
$$E_y|_{j+\frac{1}{2},k}^{n+\frac{1}{2}} \sim \frac{E_y|_{j+\frac{1}{2},k}^{n+1} + E_y|_{j+\frac{1}{2},k}^{n}}{2},$$
$$E_z|_{j+\frac{1}{2},k}^{n+\frac{1}{2}} \sim \frac{1}{8}\Big(E_z|_{j+1,k-\frac{1}{2}}^{n+1} + E_z|_{j+1,k+\frac{1}{2}}^{n+1} + E_z|_{j,k+\frac{1}{2}}^{n+1} + E_z|_{j,k-\frac{1}{2}}^{n+1}$$
$$E_z|_{j+1,k-\frac{1}{2}}^{n} + E_z|_{j+1,k+\frac{1}{2}}^{n} + E_z|_{j,k+\frac{1}{2}}^{n} + E_z|_{j,k-\frac{1}{2}}^{n}\Big)$$

Finally, we shall inject the polarization terms in the third Ampere equation (13). We need to compute $(\partial_t P_x)|_{j,k+\frac{1}{2}}^{n+\frac{1}{2}}$ and $(\partial_t P_z)|_{j,k+\frac{1}{2}}^{n+\frac{1}{2}}$ from

$$(\partial_t P_d)|_{j,k+\frac{1}{2}}^{n+\frac{1}{2}} = \mathcal{N}\,\mathrm{tr}(\mu_d \mathrm{R}(\rho|_{j,k+\frac{1}{2}}^{n+\frac{1}{2}})) - \frac{i\mathcal{N}}{\hbar}\mathrm{tr}(\mu_d [V|_{j,k+\frac{1}{2}}^{n+\frac{1}{2}}, \rho|_{j,k+\frac{1}{2}}^{n+\frac{1}{2}}]),\ d \in \{x,z\}.$$

The following approximation gives the dipolar matrix

$$\rho|_{j,k+\frac{1}{2}}^{n+\frac{1}{2}} \sim \frac{\rho|_{j,k+1}^{n+\frac{1}{2}} + \rho|_{j,k}^{n+\frac{1}{2}}}{2}.$$

To compute the potential $V|_{j,k+\frac{1}{2}}^{n+\frac{1}{2}} = -\mu_x E_x|_{j,k+\frac{1}{2}}^{n+\frac{1}{2}} - \mu_y E_y|_{j,k+\frac{1}{2}}^{n+\frac{1}{2}} - \mu_z E_z|_{j,k+\frac{1}{2}}^{n+\frac{1}{2}}$, we use

$$\begin{aligned}
E_z|_{j,k+\frac{1}{2}}^{n+\frac{1}{2}} &\sim \frac{E_z|_{j,k+\frac{1}{2}}^{n+1} + E_y|_{j,k+\frac{1}{2}}^{n}}{2},\\
E_x|_{j,k+\frac{1}{2}}^{n+\frac{1}{2}} &\sim \frac{E_x|_{j,k+1}^{n+1} + E_x|_{j,k}^{n+1} + E_x|_{j,k+1}^{n} + E_x|_{j,k}^{n}}{4},\\
E_y|_{j,k+\frac{1}{2}}^{n+\frac{1}{2}} &\sim \frac{1}{8}\Big(E_y|_{j+\frac{1}{2},k+1}^{n+1} + E_y|_{j+\frac{1}{2},k}^{n+1} + E_y|_{j-\frac{1}{2},k+1}^{n+1} + E_y|_{j-\frac{1}{2},k}^{n+1}\\
&\qquad E_y|_{j+\frac{1}{2},k+1}^{n} + E_y|_{j+\frac{1}{2},k}^{n} + E_y|_{j-\frac{1}{2},k+1}^{n} + E_y|_{j-\frac{1}{2},k}^{n}\Big).
\end{aligned}$$

Thus, we have shown how to compute the polarization term involved in the Ampere equations, using approximations of order 2 in space and time.

## 3.4 Final scheme

Finally, we need to replace the time-derivatives of the polarization **P** by their expressions (obtained in Section 3.3) in the Ampere equations (11), (12) and (13).

To simplify the expressions, let us introduce the following notations

$$T_d = \mathcal{N}\,\mathrm{tr}\,(\mu_d \mathrm{R}(\rho)),\ d \in \{x,y,z\},$$

$$T_{d_1,d_2} = \frac{i\mathcal{N}}{\hbar}\mathrm{tr}\,(\mu_{d_1}[\mu_{d_2},\rho]),\ d_1,d_2 \in \{x,y,z\}.$$

The first equation (11) on $E_x$ is,

$$\begin{aligned}
E_x|_{j,k}^{n+1} = \quad & E_x|_{j,k}^{n} + \frac{\delta t}{\mu_0}\eta_{xx}\left[(\mathbb{D}^y B_z)_{j,k}^{n+\frac{1}{2}} - (\mathbb{D}^z B_y)_{j,k}^{n+\frac{1}{2}}\right]\\
& - \frac{\delta t}{\mu_0}\eta_{xz}\frac{(\mathbb{D}^y B_x)_{j,k+\frac{1}{2}}^{n+\frac{1}{2}} + (\mathbb{D}^y B_x)_{j,k-\frac{1}{2}}^{n+\frac{1}{2}}}{2}\\
& - \eta_{xx}\delta t(\partial_t P_x)|_{j,k}^{n+\frac{1}{2}} - \eta_{xz}\delta t(\partial_t P_z)|_{j,k}^{n+\frac{1}{2}}.
\end{aligned} \tag{16}$$

From Section 3.3, we know that

$$\begin{aligned}
(\partial_t P_x)|_{j,k}^{n+\frac{1}{2}} =& T_x|_{j,k}^{n+\frac{1}{2}} + \frac{E_y|_{j-\frac{1}{2},k}^{n+1} + E_y|_{j+\frac{1}{2},k}^{n+1} + E_y|_{j+\frac{1}{2},k}^{n} + E_y|_{j-\frac{1}{2},k}^{n}}{4} T_{x,y}|_{j,k}^{n+\frac{1}{2}},\\
&+ \frac{E_z|_{j,k+\frac{1}{2}}^{n+1} + E_z|_{j,k-\frac{1}{2}}^{n+1} + E_z|_{j,k+\frac{1}{2}}^{n} + E_z|_{j,k-\frac{1}{2}}^{n}}{4} T_{x,z}|_{j,k}^{n+\frac{1}{2}},
\end{aligned}$$

and

$$(\partial_t P_z)|_{j,k}^{n+\frac{1}{2}} = T_z|_{j,k}^{n+\frac{1}{2}} + \frac{E_x|_{j,k}^{n+1} + E_x|_{j,k}^{n}}{2} T_{z,x}|_{j,k}^{n+\frac{1}{2}}, + \frac{E_y|_{j-\frac{1}{2},k}^{n+1} + E_y|_{j+\frac{1}{2},k}^{n+1} + E_y|_{j+\frac{1}{2},k}^{n} + E_y|_{j-\frac{1}{2},k}^{n}}{4} T_{z,y}|_{j,k}^{n+\frac{1}{2}}.$$

Collecting the above equations, we obtain

$$\begin{aligned} E_x|_{j,k}^{n+1} &= \frac{1}{(1+\frac{1}{2}\eta_{xz}\delta t T_{z,x}|^{n+\frac{1}{2}})} \left[ \gamma_x|_{j,k}^{n+1} - \eta_{xx}\delta t \frac{(\mathbb{A}^z E_z)_{j,k}^{n+1}}{2} T_{x,z}|_{j,k}^{n+\frac{1}{2}} \right. \\ &\quad \left. -\delta t(\eta_{xx} T_{x,y}|_{j,k}^{n+\frac{1}{2}} + \eta_{xz} T_{z,y}|_{j,k}^{n+1}) \frac{(\mathbb{A}^y E_y)_{j,k}^{n+1}}{2} \right], \end{aligned} \tag{17}$$

where $\gamma_x|_{j,k}^{n+1}$ depends only on terms computed before time $t^{n+1}$. Its expression is

$$\begin{aligned} \gamma_x|_{j,k}^{n+1} = E_x|_{j,k}^{n} &+ \frac{\delta t}{\mu_0}\eta_{xx}\left[(\mathbb{D}^y B_z)_{j,k}^{n+\frac{1}{2}} - (\mathbb{D}^z B_y)_{j,k}^{n+\frac{1}{2}}\right] - \frac{\delta t}{\mu_0}\eta_{xz}\frac{(\mathbb{D}^y B_x)_{j,k+\frac{1}{2}}^{n+\frac{1}{2}} + (\mathbb{D}^y B_x)_{j,k-\frac{1}{2}}^{n+\frac{1}{2}}}{2} \\ &- \eta_{xx}\delta t\left[T_x|_{j,k}^{n+\frac{1}{2}} + \frac{(\mathbb{A}^y E_y)_{j,k}^{n}}{2} T_{x,y}|_{j,k}^{n+\frac{1}{2}} + \frac{(\mathbb{A}^z E_z)_{j,k}^{n}}{2} T_{x,z}|_{j,k}^{n+\frac{1}{2}}\right] \\ &- \eta_{xz}\delta t\left[T_z|_{j,k}^{n+\frac{1}{2}} + \frac{E_x|_{j,k}^{n}}{2} T_{z,x}|_{j,k}^{n+\frac{1}{2}} + \frac{(\mathbb{A}^y E_y)_{j,k}^{n}}{2} T_{z,y}|_{j,k}^{n+\frac{1}{2}}\right]. \end{aligned}$$

For the second coordinate of the electric field, we obtain

$$\begin{aligned} E_y|_{j+\frac{1}{2},k}^{n+1} &= \gamma_y^{n+1} - \eta_{yy}\delta t \frac{(\mathbb{A}^y E_x)_{j+\frac{1}{2},k}^{n+1}}{2} T_{y,x}|_{j+\frac{1}{2},k}^{n+\frac{1}{2}} \\ &\quad -\eta_{yy}\delta t \frac{(\mathbb{A}^{y,z} E_z)_{j+\frac{1}{2},k}^{n+1}}{2} T_{y,z}|_{j+\frac{1}{2},k}^{n+\frac{1}{2}}, \end{aligned} \tag{18}$$

where $\gamma_y|_{j+\frac{1}{2},k}^{n+1}$ is given by

$$\begin{aligned} \gamma_y|_{j+\frac{1}{2},k}^{n+1} &= E_y|_{j+\frac{1}{2},k}^{n} + \frac{\delta t}{\mu_0}\eta_{yy}(\mathbb{D}^z B_x)_{j+\frac{1}{2},k}^{n+\frac{1}{2}} \\ &\quad -\eta_{yy}\delta t\left[T_y|_{j+\frac{1}{2},k}^{n+\frac{1}{2}} + \frac{(\mathbb{A}^y E_x)_{j+\frac{1}{2},k}^{n}}{2} T_{y,x}|_{j+\frac{1}{2},k}^{n+\frac{1}{2}} \right. \\ &\quad \left. + \frac{(\mathbb{A}^{y,z} E_z)_{j+\frac{1}{2},k}^{n}}{2} T_{y,z}|_{j+\frac{1}{2},k}^{n+\frac{1}{2}}\right], \end{aligned}$$

and depends only on variables computed before time $t^{n+1}$.

After replacing the time-derivatives of the polarization **P** in equation (13), we obtain

$$E_z|_{j,k+\frac{1}{2}}^{n+1} = \frac{1}{1+\frac{1}{2}\eta_{zx}\delta t T_{x,z}|_{j,k+\frac{1}{2}}^{n+\frac{1}{2}}} \left[ \gamma_z|_{j+\frac{1}{2},k}^{n+1} - \eta_{zz}\delta t \frac{(\mathbb{A}^z E_x)_{j,k+\frac{1}{2}}^{n+1}}{2} T_{z,x}|_{j,k+\frac{1}{2}}^{n+\frac{1}{2}} - \delta t \frac{(\mathbb{A}^{y,z}E_y)_{j,k+\frac{1}{2}}^{n+1}}{2} (\eta_{zx} T_{x,y}|_{j,k+\frac{1}{2}}^{n+\frac{1}{2}} + \eta_{zz} T_{z,y}|_{j,k+\frac{1}{2}}^{n+\frac{1}{2}}) \right], \tag{19}$$

where

$$\begin{aligned}
\gamma_z|_{j,k+\frac{1}{2}}^{n+1} =& E_z|_{j,k+\frac{1}{2}}^{n} - \frac{\delta t \eta_{zz}}{\mu_0} (\mathbb{D}^y B_x)_{j,k+\frac{1}{2}}^{n+\frac{1}{2}} - \frac{\delta t}{\mu_0}\eta_{zx} \left[ \frac{B_y|_{j,k+\frac{3}{2}}^{n+\frac{1}{2}} - B_y|_{j,k-\frac{1}{2}}^{n+\frac{1}{2}}}{2\delta z} \right] \\
&+ \frac{\delta t \eta_{zx}}{\mu_0} \frac{(\mathbb{D}^y B_z)_{j,k+1}^{n+\frac{1}{2}} + (\mathbb{D}^y B_z)_{j,k}^{n+\frac{1}{2}}}{2} \\
&- \eta_{zx}\delta t \left[ T_x|_{j,k+\frac{1}{2}}^{n+\frac{1}{2}} + \frac{E_z|_{j,k+\frac{1}{2}}^{n}}{2} T_{x,z}|_{j,k+\frac{1}{2}}^{n+\frac{1}{2}} + \frac{(\mathbb{A}^{y,z}E_y)_{j,k+\frac{1}{2}}^{n}}{2} T_{x,y}|_{j,k+\frac{1}{2}}^{n+\frac{1}{2}} \right] \\
&- \eta_{zz}\delta t \left[ T_z|_{j,k+\frac{1}{2}}^{n+\frac{1}{2}} + \frac{(\mathbb{A}^z E_x)_{j,k+\frac{1}{2}}^{n}}{2} T_{z,x}|_{j,k+\frac{1}{2}}^{n+\frac{1}{2}} + \frac{1}{2}(\mathbb{A}^{y,z}E_y)_{j,k+\frac{1}{2}}^{n+1} T_{z,y}|_{j,k+\frac{1}{2}}^{n+\frac{1}{2}} \right].
\end{aligned}$$

**Proposition 1** The discretization scheme given by equations (8), (17), (18), (19) and (14) is of order two.

If the three coordinates of the electric field $\mathbf{E}^n$ are collected in one big vector (of size $3 \times M_y \times M_z$ where we denote by $M_y$ the number of points of the grid in the direction $y$ and $M_z$ in the direction $M_z$), the three equations (17), (18) and (19) can be rewritten as a linear system.

$$\mathcal{E}^{n+1} = A\mathcal{E}^{n+1} + \mathbf{B}^n, \tag{20}$$

where the vector $\mathbf{B}^n$ depend on $\mathcal{E}^n$ and is obtained from the variables $\gamma$. This linear system is not trivial to solve as the matrix $M = \mathrm{I} - A$ is neither diagonal nor trigonal. However, the matrix is sparse, each of its rows contains less than 7 non vanishing coefficients.

To solve the linear system (20), we use a GMRES method implemented in [3, 4]. Hence, we obtain $\mathcal{E}^{n+1} = (\mathrm{I} - A)^{-1}\mathbf{B}^n$, which contains the electric field **E** on the domain at time $t^{n+1}$.

# 4 Boundary Conditions

The equations describing the propagation of a laser pulse in our medium are then fully discretized.

We consider that before traveling through the medium, the wave-field propagates in a linear medium (as shown in Figure 1), whose index is chosen to minimize the reflexion at the interfaces. This greatly simplifies the boundary conditions and the introduction of an incident wave.

## 4.1 Boundary conditions in the direction of propagation

To approach the physical conditions, in which the boundaries are transparent for the wave, we shall use the classical Silver-Müller condition [17] as in the unidimensional case [14]. We denote by $\tilde{c}$ the speed of light in the linear medium.

The interfaces at the entry and the exit of the domain (see Figure 1) are represented in Figure 3, where the first point of the grid along the direction $z$ is denoted by 1 and the last one by $M_z$.

Figure 3: Boundary conditions in the direction of propagation $z$.

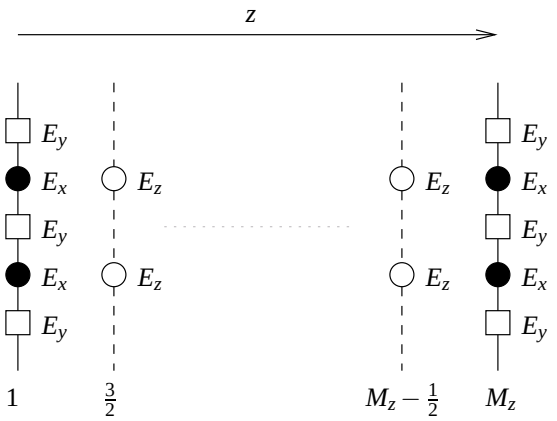


At the domain entry, the Silver-Müller condition is written:

$$(\mathbf{E} - \mathbf{E}^i) \times \mathbf{n} - \tilde{c}((\mathbf{B} - \mathbf{B}^i) \times \mathbf{n}) \times \mathbf{n} = 0,$$

where $(\mathbf{E}_i, \mathbf{B}_i)$ is the incident electromagnetic wave and $\mathbf{n}$ the outer normal vector to the domain.

At the domain exit, the condition becomes

$$\mathbf{E} \times \mathbf{n} - \tilde{c}(\mathbf{B} \times \mathbf{n}) \times \mathbf{n} = 0.$$

By detailing for each coordinate it gives

$$-E_y + E_y^i + \tilde{c}(B_x - B_x^i) = 0, \tag{21}$$
$$E_x - E_x^i + \tilde{c}(B_y - B_y^i) = 0, \tag{22}$$

for the entry and

$$E_y + \tilde{c}B_x = 0, \tag{23}$$
$$E_x - \tilde{c}B_y = 0, \tag{24}$$

for the exit.

In a first step, let us discretize equation (21) for the time $t^{n+1}$ and the points $(j-\frac{1}{2},\frac{3}{2})\ \forall j$. We get

$$-\frac{1}{2}\left(E_y|^{n+1}_{j-\frac{1}{2},1} + E_y|^{n+1}_{j-\frac{1}{2},2}\right) + \frac{\tilde{c}}{2}\left(B_x|^{n+\frac{3}{2}}_{j-\frac{1}{2},\frac{3}{2}} + B_x|^{n+\frac{1}{2}}_{j-\frac{1}{2},\frac{3}{2}}\right) = \tilde{c}B_x^i|^{n+1}_{j-\frac{1}{2},\frac{3}{2}} - E_y^i|^{n+1}_{j-\frac{1}{2},\frac{3}{2}}.$$

In order to compute $B_x|^{n+\frac{3}{2}}_{j-\frac{1}{2},\frac{3}{2}}$, we use the Faraday equation

$$\begin{aligned} B_x|^{n+\frac{3}{2}}_{j-\frac{1}{2},\frac{3}{2}} =& B_x|^{n+\frac{1}{2}}_{j-\frac{1}{2},\frac{3}{2}} - \frac{\delta t}{\delta y}(E_z|^{n+1}_{j,\frac{3}{2}} - E_z|^{n+1}_{j-1,\frac{3}{2}}) \\ &+ \frac{\delta t}{\delta z}(E_y|^{n+1}_{j-\frac{1}{2},2} - E_y|^{n+1}_{j-\frac{1}{2},1}), \end{aligned}$$

which yields

$$\begin{aligned} E_y|^{n+1}_{j-\frac{1}{2},1} =& \frac{1}{1+\tilde{c}\frac{\delta t}{\delta z}}\left(2\tilde{c}B_x|^{n+\frac{1}{2}}_{j-\frac{1}{2},\frac{3}{2}} - 2\tilde{c}B_x^i|^{n+1}_{j-\frac{1}{2},\frac{3}{2}} + 2E_y^i|^{n+1}_{j-\frac{1}{2},\frac{3}{2}}\right) \\ &+ \frac{1}{1+\tilde{c}\frac{\delta t}{\delta z}}\left(-\tilde{c}\frac{\delta t}{\delta y}(E_z|^{n+1}_{j,\frac{3}{2}} - E_z|^{n+1}_{j-1,\frac{3}{2}}) - (1-\tilde{c}\frac{\delta t}{\delta z})E_y|^{n+1}_{j-\frac{1}{2},2}\right). \end{aligned}$$

The equation (24) is written for time $t^{n+1}$ and the points $(j,\frac{3}{2}),\ \forall j$:

$$\frac{1}{2}\left(E_x|^{n+1}_{j,1} + E_x|^{n+1}_{j,2}\right) + \frac{\tilde{c}}{2}\left(B_y|^{n+\frac{3}{2}}_{j,\frac{3}{2}} + B_y|^{n+\frac{1}{2}}_{j,\frac{3}{2}}\right) = E_x^i|^{n+1}_{j,\frac{3}{2}} + \tilde{c}B_y^i|^{n+1}_{j,\frac{3}{2}}.$$

The Faraday equations give

$$B_y|^{n+\frac{3}{2}}_{j,\frac{3}{2}} = B_y|^{n+\frac{1}{2}}_{j,\frac{3}{2}} - \frac{\delta t}{\delta z}(E_x|^{n+1}_{j,2} - E_x|^{n+1}_{j,1}).$$

Finally, $E_x|^{n+1}_{j,1}$ is computed by the equation

$$E_x|^{n+1}_{j,1} = \frac{1}{1+\tilde{c}\frac{\delta t}{\delta z}}\left(-2\tilde{c}B_y|^{n+\frac{1}{2}}_{j,\frac{3}{2}} + 2E_x^i|^{n+1}_{j,\frac{3}{2}} + 2\tilde{c}B_y^i|^{n+1}_{j,\frac{3}{2}}\right) - \frac{1-\tilde{c}\frac{\delta t}{\delta z}}{1+\tilde{c}\frac{\delta t}{\delta z}}E_x|^{n+1}_{j,2}.$$

Using the same method, we can express the conditions at the exit of the domain:

$$E_y|^{n+1}_{j-\frac{1}{2},M_z} = -\frac{1-\frac{\tilde{c}\delta t}{\delta z}}{1+\frac{\tilde{c}\delta t}{\delta z}} E_y|^{n+1}_{j-\frac{1}{2},M_z-1} - \frac{2\tilde{c}}{1+\frac{\tilde{c}\delta t}{\delta z}} B_x|^{n+\frac{1}{2}}_{j-\frac{1}{2},M_z-\frac{1}{2}} + \frac{\frac{\tilde{c}\delta t}{\delta y}}{1+\frac{\tilde{c}\delta t}{\delta z}} (E_z|^{n+1}_{j,M_z-\frac{1}{2}} - E_z|^{n+1}_{j-1,M_z-\frac{1}{2}}),$$

$$E_x|^{n+1}_{j,M_z} = -\frac{1-\frac{\tilde{c}\delta t}{\delta z}}{1+\frac{\tilde{c}\delta t}{\delta z}} E_x|^{n+1}_{j,M_z-1} + \frac{2\tilde{c}}{1+\frac{\tilde{c}\delta t}{\delta z}} B_y|^{n+\frac{1}{2}}_{j,M_z-\frac{1}{2}}.$$

### 4.2 Boundary conditions in the transverse direction

In the transverse direction $y$, we use periodic boundary conditions: the first and last rows of the grid are identical. As we expect to study pulses vanishing near the transverse boundaries, we take simple conditions.

That is to say, the following relations are satisfied by the variables

$$\begin{aligned} E_x(1,k) &= E_x(M_y,k), \\ E_z(1,k) &= E_z(M_y,k), \\ B_y(1,k) &= B_y(M_y,k), \\ \rho(1,k) &= \rho(M_y,k), \end{aligned}$$

where $M_y$ is the number of points of the grid in the direction $y$.

## 5 Numerical experimentations

In order to validate the scheme, let us proceed with several experimentations. In a first section, we show that the bidimensional scheme gives similar results than the unidimensional scheme [14] when the wave-field does not depend on the variable $y$. Finally, we study the light propagation in a KDP crystal. The dipolar matrix $\mu$ describing the KDP crystal is given in [5]. The corresponding model has 5 states and the lower energy state is 3-fold degenerate. It can be used to study harmonic generation.

In the sequel, we highlight several physical effects that a bidimensional model can render contrary to a unidimensional model.

For instance, we can now take the diffraction into account when studying laser propagation. The effect of diffraction on a very thin laser beam is represented in Figure 4. The incoming wave is a $1.06\,\mu$m and 20 fs Gaussian pulse polarized in the direction $y$ (see Figure 1). Its width is $0.5\,\mu$m. The peak-amplitude of the pulse is $10^6\,\mathrm{V/m}$. For this run, we take 100 points per wave-length in the direction $z$

and 20 in the direction $y$. The time-step is given by $\tilde{c}\delta t\sqrt{\frac{1}{\delta z^2}+\frac{1}{\delta y^2}}=0.75$, where $\tilde{c}$ is the speed of light in the linear medium ($\tilde{c}=0.826\%\, c_0$).

Figure 4: Amplitude of the electric field (in V/m) of a very thin ($\frac{1}{2}\,\mu$m) laser beam after a short propagation (under $4\,\mu$m) in a KDP crystal.

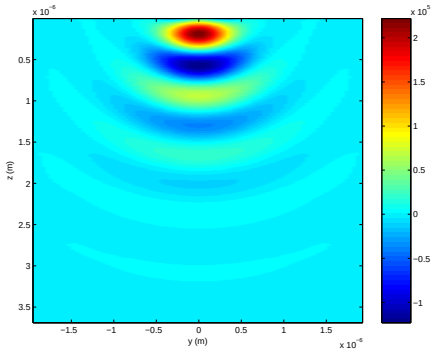


However, this is a pure linear effect and this phenomenon could have been studied with a classical Yee scheme without the polarization term.

## 5.1 Reduction to the unidimensional case

In this section, we consider the case when the electric field **E** and the magnetic induction **B** do not depend on the second variable in space $y$. We should obtain results close to those obtained from the unidimensional scheme described in [14]. We run an experiment of second harmonic generation. For an explanation of second harmonic generation, one can see, for instance, Chapter 2 of [8]. The incoming wave is a 20 fs Gaussian pulse of $10^8\,\mathrm{V/m}$ polarized along the direction $y$ at the phase matching angle. Numerically, we choose to take 100 points per wave-length in space in the directions $y$ and $z$, the time-step is computed to ensure the CFL condition (which yields different time-steps for the two schemes). Hence, we take the time step $\delta t$ such that $\tilde{c}\delta t\sqrt{\frac{1}{\delta z^2}+\frac{1}{\delta y^2}}=0.75<1$, where $\tilde{c}$ is the speed of light in the medium, $\delta y$ and $\delta z$ the two space steps.

Let us recall that even harmonics should appear in the component $E_x$ of the electric field and odd harmonics in $E_y$. In Figures 5 and 6, we have plotted the evolution (in space) of the two components $E_x$ and $E_y$ for both schemes.

Figure 5: Evolution of the component $E_y$ for both schemes.

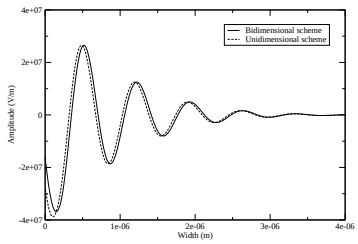


Figure 6: Evolution of the component $E_x$ for both schemes.

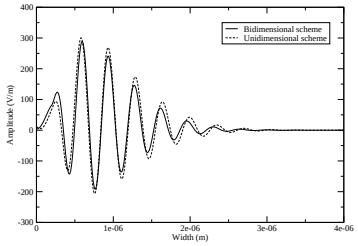


The results given by the two different schemes are in good agreement. The results obtained by the bidimensional scheme do not depend of the point chosen in the direction $y$.

## 5.2 Second Harmonic Generation in a KDP crystal

In this section, we study second harmonic generation in a KDP crystal with our complete bidimensional model. We use the dipolar matrix given in [5], which describes rather accurately a KDP crystal.

The incoming wave is a 20 fs Gaussian pulse of $1.5 \times 10^9 \mathrm{V/m}$ at the wave-length $1.06\,\mu$m propagating in a $20\,\mu$m KDP crystal.

The electric field **E** is polarized along the $y$-axis (see Figure 1). The second harmonic wave and all harmonics of even order should appear in the $x$-axis. Cubic harmonic and higher odd harmonics should also be observed along the $y$-axis.

In this run, we take 125 points per wave-length along the direction $z$. The space step in the direction $y$ is given by $\delta y = 85\delta z$ (the grid has 400 points in the direction $y$). The time step $\delta t$ is given by $\delta t = 0.75\tilde{c}\frac{1}{\sqrt{\frac{1}{\delta z^2}+\frac{1}{\delta y^2}}}$, using the same notations as in the previous section.

Figure 7 shows a snapshot of the two components of the electric field after a $20\,\mu$m propagation in the crystal. As the wave propagates through the crystal, the intensity of the component $E_x$ is increasing. One can also observe the thickness of $E_x$ compared to $E_y$: second-harmonic generation could be used to increase the contrast of a pulse.

Figure 7: Amplitude of the electric field in V/m after a propagation of 20 $\mu$m in the crystal. The left figure represents the component $E_y$, the right one $E_x$.

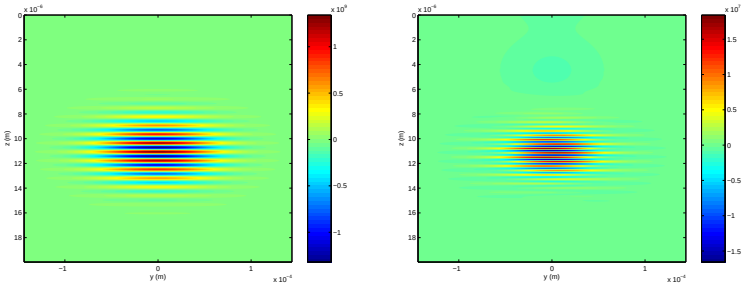


Now, we observe the evolution over time of the electric field at the center of the pulse and compare its intensity with the one computed by an unidimensional scheme. First let us represent the spectrum of the electric field, in its two components $E_y$ and $E_x$, at the center of the pulse.

Figure 8: Spectrum of the electric field for several times in arbitrary units after a propagation of 20 $\mu$m in the crystal. The left figure represents the component $E_y$, the right one $E_x$. The frequency is relative to the frequency of the incoming wave. (For the plot of $E_y$, we use dotted lines when the wave is not entirely entered in the crystal.)

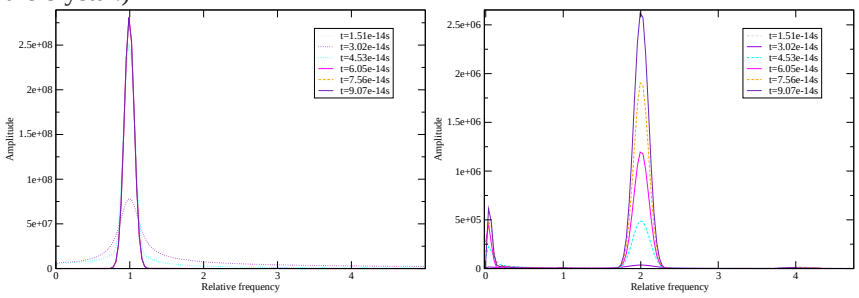


As we expected, the intensity of the second harmonic (as shown in the rightmost plot of Figure 8) is increasing as the wave travels through the crystal. We can also observe optical rectification which leads to the creation of lower frequencies. The intensity of the fundamental harmonic is also slowly decreasing as the pulse propagates (as the length of propagation is short, this effect is rather difficult to observe in Figure 8).

At the center of the pulse, the intensity of the electric field **E** computed by the bidimensional scheme is identical to the one computed with the unidimensional scheme [14]. This is also in good agreement with physical experiments (see [14]).

In the unidimensional case, at the phasing matching angle, the component $E_x$ contains only even harmonics. In the bidimensional case, this is no longer the case. In Figure 5.2, we have plotted the component $E_x$ after a short propagation of the crystal. The evolution of $E_x$ for four different points in the direction $y$ is represented on the right part of the figure.

Figure 9: Evolution of $E_x$ far from the center ($y = 0$) of the pulse for the points $y = 2.8832 \times 10^{-5}$m, $5.7664 \times 10^{-5}$m, $8.6496 \times 10^{-5}$m and $11.5328 \times 10^{-5}$m (from the left to the right, the top to the bottom). For the rightmost pictures, the X-coordinate represents the width in meters (in the direction $z$) and the Y-coordinate the amplitude of the field in V/m.

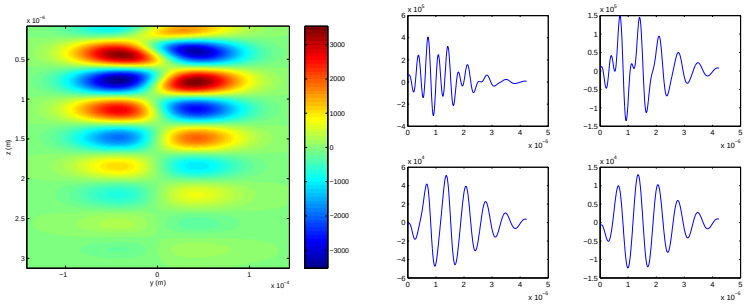

In Figure 5.2, we can see that the shape of the component is not Gaussian as it would have been with the unidimensional model. Far from the center of the pulse, the component $E_x$ is mainly composed of the same frequencies as the incoming wave. This comes from the term $\partial_y B_z$ involved in the first equation of the system (3). This term is vanishing in the unidimensional case. For short distances of propagation, the nonlinearity introduced in (3) is negligible before this linear effect.

Another difference between the two models can also be observed if we consider electric field of higher intensities. In Figure 10, we show the results of running the same experiment but with an intensity of $10^{10}\,\mathrm{V/m}$. The left part of the figure represents the component $E_x$ at the center computed with a bidimensional scheme and the right one the result obtained from the unidimensional scheme [14].

Figure 10: Evolution of the component $E_x$ for both schemes. The left plot represents the amplitude computed by the bidimensional scheme, the right one the amplitude computed by the unidimensional scheme.

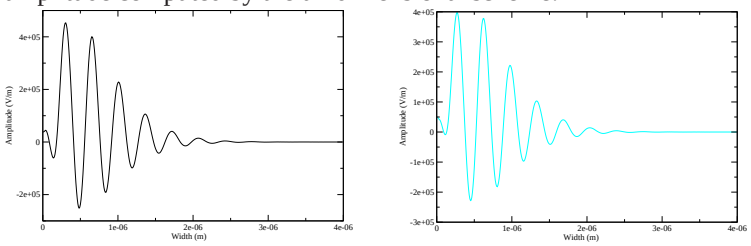


The intensity computed by the bidimensional scheme is slightly higher than the intensity computed by the unidimensional case. This could be an effect of the focusing of the beam. Indeed, the unidimensional scheme can not render this effect also known as the Kerr effect. The Kerr effect increases the intensity of the pulse at its center, thus increasing the efficiency of the second harmonic generation. However, after a longer distance of propagation this cubic effect disturbs the phase matching and decreases the efficiency of the conversion (see [16]).

# 6 Conclusion

In this paper, we have shown how to extend the scheme described in [14] to the bidimensional case. Thus we are able to study new physicals effects acting on the shape of the laser beam.

However, the accuracy of this microscopic model has a rather high numerical cost. This model is not suitable for long distance of propagation. Nonetheless, the computation times can be significantly reduced thanks to parallelization (with MPI [9, 10]). This has been studied in [13], the domain of each processor [1] is decomposed in the transverse direction. In the Bloch equations, the space variables act as parameters so the equations can be solved for each point in space in parallel. Thus we have observed a quasi-linear speedup of the solving of the Bloch equations with the number of processors. As the equations on the electric field **E** and the magnetic induction **B** are not written in the same points in time, the Yee scheme is easy to parallelize. Thanks to the library [3], the solving of the Maxwell equations with the polarization part can also be parallelized. Hence, we were able to parallelize the entire solving of the Maxwell-Bloch model. The speedup for this entire solving is far from being optimal, this parallelization is still a work-in-progress.

## Acknowledgments

The author wishes to express his sincere thanks to Christophe Besse, Antoine Bourgeade and Pierre Degond for their help throughout this work.

## References

[1] V. Kumar A. Grama and A. Gupta. *Introduction to Parallel Computing*. Addison-Wesley, second edition, 2003.

[2] H.J. Bakker, P.C.M. Planken, and H.G. Muller. Numerical calculation of optical frequency-conversion processes: a new approach. *J. Opt. Soc. Am. B*, 6(9):1665–1672, 1989.

[3] Satish Balay, Kris Buschelman, William D. Gropp, Dinesh Kaushik, Matt Knepley, Lois Curfman McInnes, Barry F. Smith, and Hong Zhang. PETSc home page. http://www.mcs.anl.gov/petsc, 2001.

[4] Satish Balay, Kris Buschelman, William D. Gropp, Dinesh Kaushik, Matt Knepley, Lois Curfman McInnes, Barry F. Smith, and Hong Zhang. PETSc users manual. Technical Report ANL-95/11 - Revision 2.1.5, Argonne National Laboratory, 2002.

[5] C. Besse, B. Bidégaray, A. Bourgeade, P. Degond, and O. Saut. A Maxwell-Bloch model with discrete symmetries for wave propagation in nonlinear crystals: an application to KDP. *M2AN Math. Model. Numer. Anal.*, 38(2):321–344, 2004.

[6] A. Bourgeade and E. Freysz. Computational modeling of second-harmonic generation by solution of full-wave vector Maxwell equations. *J. Opt. Soc. Am. B*, 17(2):226–234, 2000.

[7] A. Bourgeade and O. Saut. Comparison of macroscopic and microscopic models for ultrashort pulses propagation in nonlinear crystals. submitted, 2004.

[8] Robert W. Boyd. *Nonlinear Optics*. Academic Press, 1992.

[9] W. Gropp, E. Lusk, N. Doss, and A. Skjellum. A high-performance, portable implementation of the MPI message passing interface standard. *Parallel Computing*, 22(6):789–828, September 1996.

[10] William D. Gropp and Ewing Lusk. *User's Guide for* `mpich`*, a Portable Implementation of MPI*. Mathematics and Computer Science Division, Argonne National Laboratory, 1996. ANL-96/6.

[11] Alan C. Newell and Jerome V. Moloney. *Nonlinear optics*. Advanced Topics in the Interdisciplinary Mathematical Sciences. Addison-Wesley Publishing Company Advanced Book Program, Redwood City, CA, 1992.

[12] R. Maleck Rassoul, A. Ivanov, E. Freysz, A. Ducasse, and F. Hache. Second-harmonic generation under phase-velocity and group-velocity mismatch: influence of cascading self-phase and cross-phase modulation. *Opt. Lett.*, 22(5):268–270, 1997.

[13] Olivier Saut. *Étude numérique des nonlinéarités d'un cristal par résolution des équations de Maxwell-Bloch*. PhD thesis, INSA Toulouse, 2003.

[14] Olivier Saut. Computational modeling of ultrashort powerful laser pulses in an anisotropic crystal. *J. Comput. Phys.*, 197(2):624–646, 2004.

[15] Leonard I. Schiff. *Quantum Mechanics*. Mc Graw-Hill International Editions, 1995.

[16] D. Eimerl T. Ditmire, A.M. Rubenchik and M.D. Perry. Effects of cubic nonlinearity on frequency doubling of high-power laser pulses. *J. Opt. Soc. Am. B*, 13(4):649–655, 1995.

[17] A. Taflove and S. Hagness. *Computational electrodynamics: the finite-difference time-domain method*. Artech House Inc., Boston, MA, second edition, 2000.

[18] K. S. Yee. Numerical solution of initial boundary value problems involving Maxwell's equations in isotropic media. *IEEE Trans. Antennas Propag.*, AP-14:302–307, 1966.

# List of Figures